*Progress In Electromagnetics Research C, Vol. 86, 55–67, 2018*

# A Broadband Crossed-Slot Circularly Polarized Antenna with Stable Phase Center for GNSS Applications

**Hongliang Zhang, Yuanyue Guo*, Wenjuan Zhang, and Gang Wang**

**Abstract**—A broadband circularly polarized microstrip antenna with stable phase center is proposed for multi-mode GNSS applications. The proposed antenna consists of two crossed slots on one side of PCB and a Γ-shaped microstrip feeding structure on the other side of PCB. Measurement of the designed antenna demonstrates that a −10-dB impedance bandwidth of 76.7% and a 3-dB axial ratio bandwidth of 64% are realized, which cover all GPS, BeiDou, Galileo, and GLONASS bands ranging from 1.164 GHz to 1.612 GHz. In addition, stable phase center for orientation in the region above 10° elevation is realized for high-precision positioning. For each GNSS band, phase center variation with respect to its own mean phase center can be retained within 5°. Over the whole GNSS bands, phase center variation with respect to the common mean phase center is retained within 6°.

## 1. INTRODUCTION

Global Navigation Satellite System (GNSS) serves as a vital infrastructure in daily life by providing location, speed, and time information [1]. Nowadays, different GNSS systems have been deployed and operated on different frequency bands such as Europe's Global Satellite Navigation System (Galileo), Global Positioning System (GPS), BeiDou Navigation Satellite System (BDS), and Russia's Global Navigation Satellite System (GLONASS). As a result, a multi-mode GNSS antenna suitable for all the GNSS systems should be circularly polarized (CP) on the whole GNSS bands ranging from 1.164 GHz to 1.612 GHz, viz., from the lowest Galileo E5a/E5b band (1189.5 MHz ± 25.5 MHz) to the highest GLONASS L1 (1605 MHz ± 7 MHz) band, which indicates a relative bandwidth of 32.2%. For high-precision positioning service such as deformation measurement of the earth's crust and attitude determination, a multi-mode antenna should provide stable antenna phase center in all the GNSS bands and for all directions in the broad beam [2].

Among various wideband CP antenna configurations, printed slot-based antennas held a growing interest in recent years for GNSS applications, due to their wide operating bandwidth and easy integration with monolithic microwave-integrated circuits [3–7]. In [3], a rotated slot was deployed to realize broadband radiation, which yielded −10-dB impedance bandwidth (IBW) of 48.9%. In [4], by deploying a halberd-shaped feeding signal line and a square ring patch in the square slot, a 3-dB axial ratio bandwidth (ARBW) of more than 25.3% was realized. In [5], a compact broadband monopole-slot CP antenna was proposed by adding an asymmetric quarter-wavelength L-shaped slot on the circuit corner, which provides a 3-dB ARBW of 23%. In [6], a broadband CPW-fed CP slot antenna with 27% ARBW has been designed, which achieves circular polarization by opening the radiation slot at the lower left slot. In [7], a square slot CP antenna with asymmetric stub protruding from one side of slot was reported for C-band operation, which yielded a −10-dB IBW of about 90.2% (3.5–9.25 GHz) and 3-dB ARBW of 40% (4.6–6.9 GHz).

*Received 5 June 2018, Accepted 23 July 2018, Scheduled 29 July 2018*

* Corresponding author: Yuanyue Guo (yuanyueg@ustc.edu.cn).

The authors are with the Department of Electronic Engineering and Information Science, University of Science and Technology of China, Hefei 230027, China.

For high-precision GNSS applications, stable antenna phase center is of vital importance because the center is actually used as the reference point of receiving or transmitting, i.e., the origin of ranging in practice [8]. Unfortunately, antenna phase center is usually a function of both frequency and observing region [9]. Besides, most antennas do not hold a unique phase center but a mean phase center (MPC) over the interesting observing region. In practice, phase center variation (PCV) can be used to evaluate the stability of MPC over the observing region, which is the deviation between the real phase front and the ideal one when the antenna reference center corrected to the MPC. Therefore, for high-precision positioning, accurate MPC and low PCV are desired [2, 10]. Generally, stable phase center tends to require symmetric antenna configurations [11], which is somewhat different from the asymmetry requirement for single-fed CP antennas. In [11], a four-arm spiral traveling-wave antenna with stable phase center was reported for GPS bands, in which PCV retained within 10° above the 10° elevation space. In [12] and [13], two microstrip antennas with perfect stable phase center for BDS B1 band and BDS B3 band have been proposed, where the MPC deviation with frequency keeps below 1.19 mm and 0.75 mm over two BDS bands, respectively. Unluckily, no discussion was carried out on MPC stability over observing region. By adopting stacked patches [14], ring slot [15], fractal slot [16], crossed-dipole [17], and tilted radiating patch [18], broadband circularly polarized antennas working at GNSS bands have been proposed; however, no stress was laid on phase center stability. Therefore, achieving stable phase center in a broad beam covering all the GNSS bands for multi-mode applications is still challenging.

In this work, we propose and design a novel broadband CP antenna with stable phase center in all the GNSS bands and a broad beam, with −10-dB IBW and 3-dB ARBW reaching up to 76.7% and 64%, respectively. Due to the quasi-symmetric crossed-slot, the antenna has s stable phase center above the 10° elevation region. Meanwhile, the antenna performs constant and symmetric upper radiation patterns. This paper is organized as follows. In Section 2, antenna configuration and mean phase center determination are presented. The measured performances of the antenna are introduced in Section 3, as well as the phase response. Section 4 gives further discussion on the crossed-slot and unidirectional radiation. Finally, Section 5 concludes this paper.

## 2. ANTENNA DESIGN

### 2.1. Antenna Structure

Geometry of the proposed microstrip antenna is shown in Fig. 1. The proposed antenna consists of a microstrip feeding network and a quasi-symmetric crossed-slot etched on the PCB ground plane as radiators. The crossed slots function as a pair of orthogonal dipoles to generate the orthogonal electric field modes for circular polarization. To achieve 90° phase shift for the two orthogonal electric fields, the horizontal and vertical slots have different lengths and widths. The feeding network is a Γ-shaped strip, which is typically asymmetric and with certain offset from the symmetry axis of the crossed slots. The offset can be adjusted to modify the CP radiation. A stub is added on the back of the Γ-shaped strip for fine tuning and the stub may be used to improve the IBW and ARBW by carefully adjusting its position and dimensions. The initial values of the antenna geometry can be set by following some basic considerations. To behave as a half-wavelength dipole, the horizontal slot is set to have initial values of $W1 = 10$ mm and L1 roughly estimated by Eq. (1) where $\varepsilon_r$ and $f_L$ represent the relative permittivity of substrate and lowest CP working frequency in GHz. In order to excite orthogonal modes with 90° phase difference, initial dimensions of the vertical slot can be set different from that of the horizontal, which are 75 mm and 15 mm for L2 and W2, respectively. After implementing careful optimization in the simulation software ANSYS Electronics Desktop with the initial values, we obtain the antenna geometrical parameters as listed in Table 1.

$$L = \frac{300}{2f_L\sqrt{(1+\varepsilon_r/2)}}\,(\text{mm}) \tag{1}$$

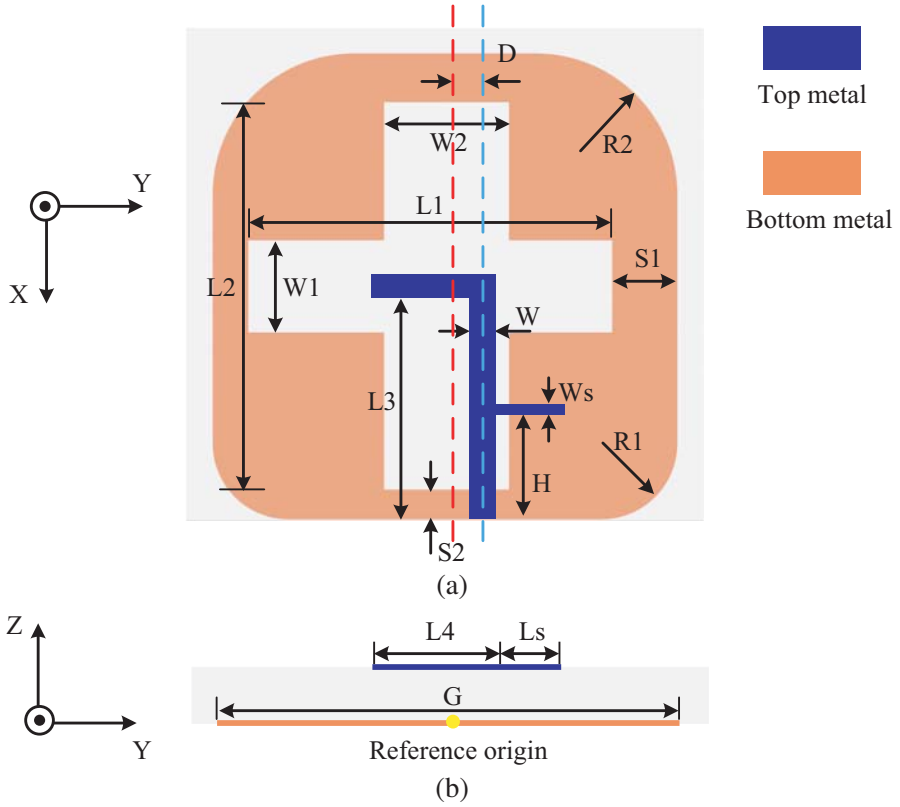


**Figure 1.** Geometry of the proposed antenna on PCB. (a) Top view and (b) side view.

**Table 1.** Dimensions of the proposed antenna (unit: mm).

| R1 | R2 | L1 | L2 | L3 | L4 | Ls | H |
|---|---|---|---|---|---|---|---|
| 14.1 | 23.9 | 68.1 | 79.1 | 42.5 | 23.4 | 10.3 | 9.9 |
| W | W1 | W2 | Ws | S1 | S2 | D | G |
| 6.5 | 17.1 | 21.2 | 1.1 | 14.7 | 3.8 | 5.8 | 90 |

### 2.2. The Determination of MPC and PCV

Determination of the MPC is a key concern. Since most antennas do not hold an ideal and unique phase center but an MPC within the interested angular region of surrounding space, an effective method to determine the MPC of antenna is desired. Several techniques for phase center estimation can be used such as spherical phase expansion computation method, edge diffraction method, and three-antenna method [2]. In this paper, we calculate the MPC by using the simulation software ANSYS Electronics Desktop.

In ANSYS Electronics Desktop, calculation of MPC can be performed without extra data post-processing. The MPC searching technique mainly includes four steps:

1) define a relative coordinate system and assign three variables for the relative coordinate origin;
2) choose phase quantity of interest and calculation angular ranges (both $\theta$ and $\varphi$), in which solid angular region is allowed. This step allows phase quantity to be re-calculated when the relative coordinate system is repositioned (changing origin defined in step 1);
3) create an optimization setup with goal to search for the MPC, where expression to be optimized is the peak-to-peak continuous angle of the phase quantity;

4) start the optimization and choose the relative origin as MPC when the corresponding cost is minimal.

The MPC is evaluated over the total region above 10° elevation. We may obtain the MPC for each GNSS band first, and then the common MPC for the GNSS bands. To denote the MPC's location, we define the reference coordinate system as shown in Fig. 1 and set its origin at the geometry center of ground plane.

After obtaining the MPC, we can determine the PCV from phase pattern by correcting the antenna reference point to the corresponding MPC. For an ideal point source antenna, phase pattern is constant when the antenna reference point corrected to the unique phase center, that is, the PCV is zero. However, for most antennas, there exists a deviation in the actual phase front from the ideal one at various angles of wave incidence, and the deviation is defined as PCV, which will cause ranging error for GNSS applications [2]. Therefore, MPC stability can be evaluated by PCV, and low PCV means stable antenna phase center over the observing region. Our goal is to design an antenna with low PCV in a broad beam covering all the GNSS bands for multi-mode applications.

### 2.3. Electric Field Distributions

To verify the CP radiation, the simulated electric field distributions of the antenna at GPS L5 (1176.45 MHz), BDS B3 (1268.52 MHz), and BDS B1 (1561.098 MHz), which represent the low, middle,

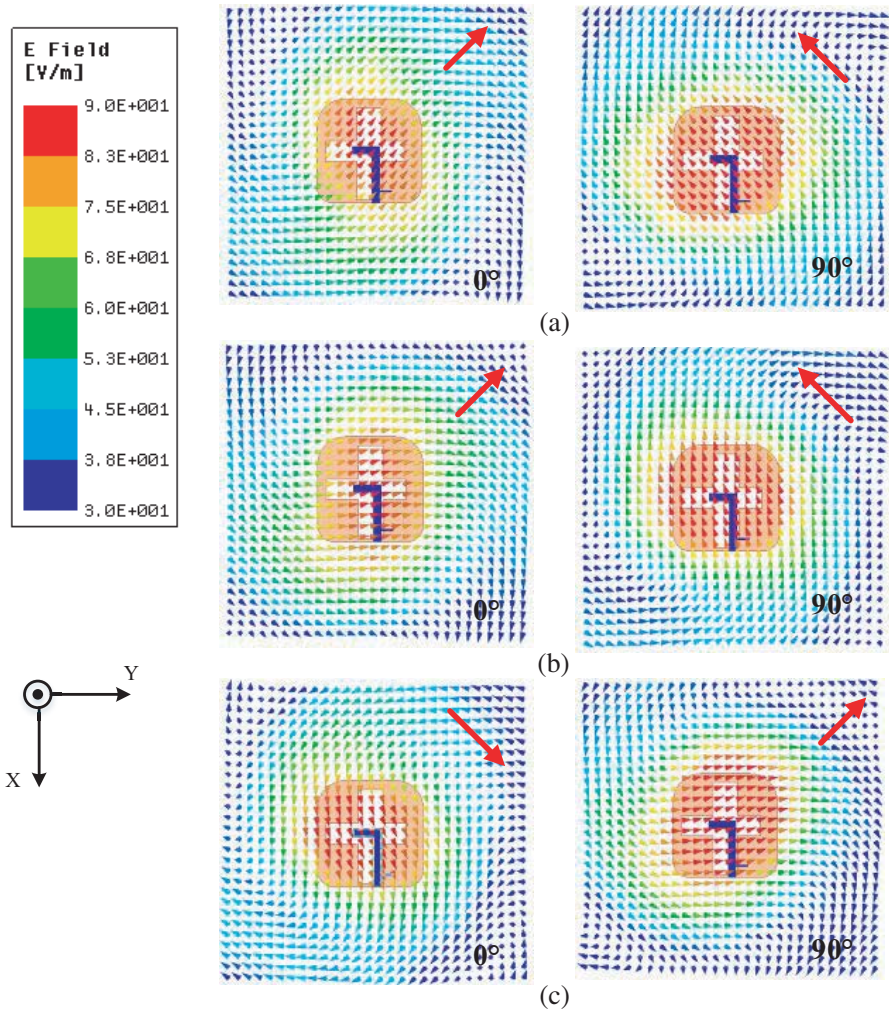


**Figure 2.** Electric field distributions at three GNSS bands. (a) GPS L5, (b) BDS B3, (c) BDS B1.

and high frequency of GNSS bands, respectively, are plotted in Fig. 2. We observe from the results that the distributions of electric field are with equal magnitude in $+Z$ direction. From $\varphi = 0°$ to $\varphi = 90°$, the total electric field as marked by red arrow, flows in clockwise direction in the $+Z$ direction, indicating the proposed antenna performs right-hand circularly polarized radiation.

## 3. PERFORMANCE OF THE PROPOSED ANTENNA

### 3.1. Antenna Bandwidth and Radiation Performance

Prototype of the designed antenna is fabricated as shown in Fig. 3. The antenna is printed on a Rogers RO4360 substrate ($\varepsilon_r = 6.15$, $\tan\delta = 0.0038$), with a size of 100 mm × 95 mm × 1.524 mm. Fig. 4(a) shows the measured and simulated $S_{11}$, where we find that −10-dB IBW can be acquired in frequency ranging from 0.9 GHz to 2.02 GHz (viz., 76.7% relative bandwidth).

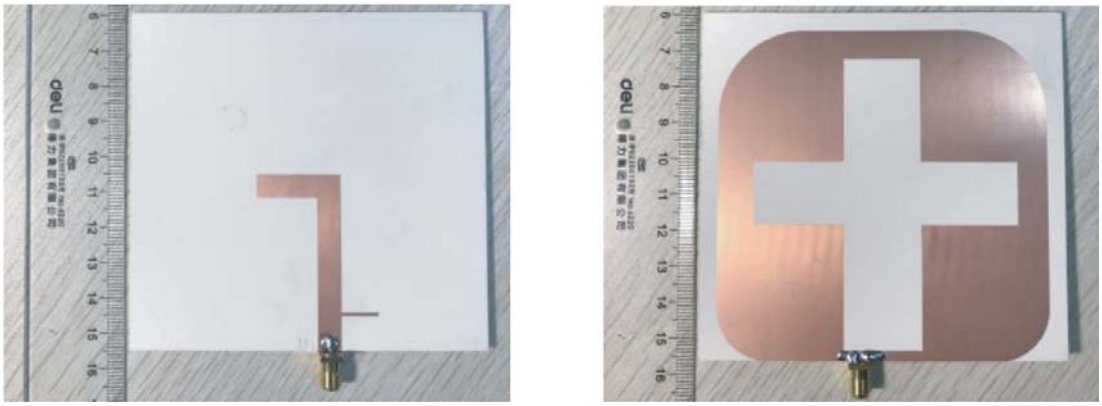

(a) (b)

**Figure 3.** Fabricated prototype of the proposed antenna. (a) Top view, (b) bottom view.

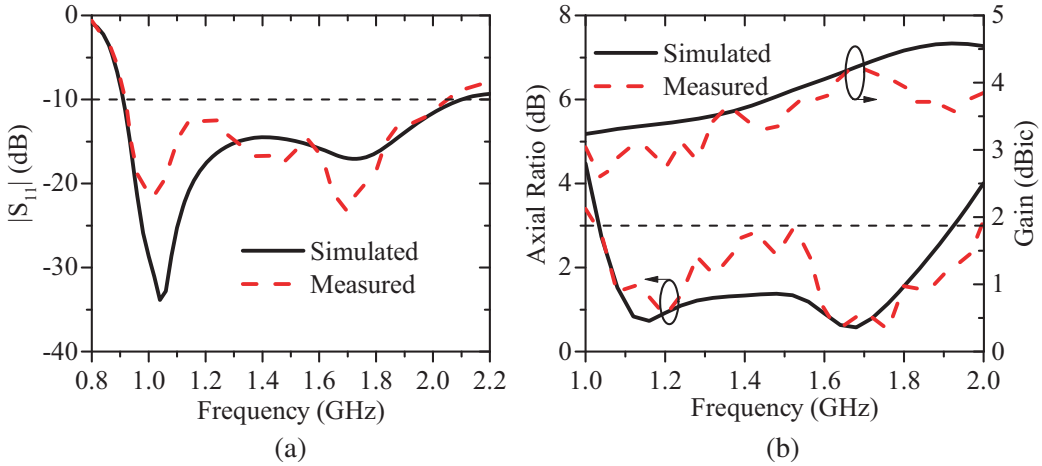


**Figure 4.** (a) Simulated and measured $S_{11}$. (b) Simulated and measured axial ratio and gain.

Figure 4(b) shows the simulated and measured gains and 3-dB ARBW of the antenna. We find that the measured 3-dB ARBW can be acquired in frequency ranging from 1.03 GHz to 2.0 GHz (viz., 64% relative bandwidth), covering the whole GNSS bands (from 1.164 GHz to 1.612 GHz). At the same time, we can observe from Fig. 4(b) that there are some discrepancies between the simulated and measured axial ratio results, especially from 1.3 GHz to 1.5 GHz. This is possibly caused by the experimental

environment, such as the feeding coaxial line, from which the parasitic radiation may affect the axial ratio measurement, whereas, please note that the axial ratio keeps below 3 dB from 1.3 GHz to 1.5 GHz.

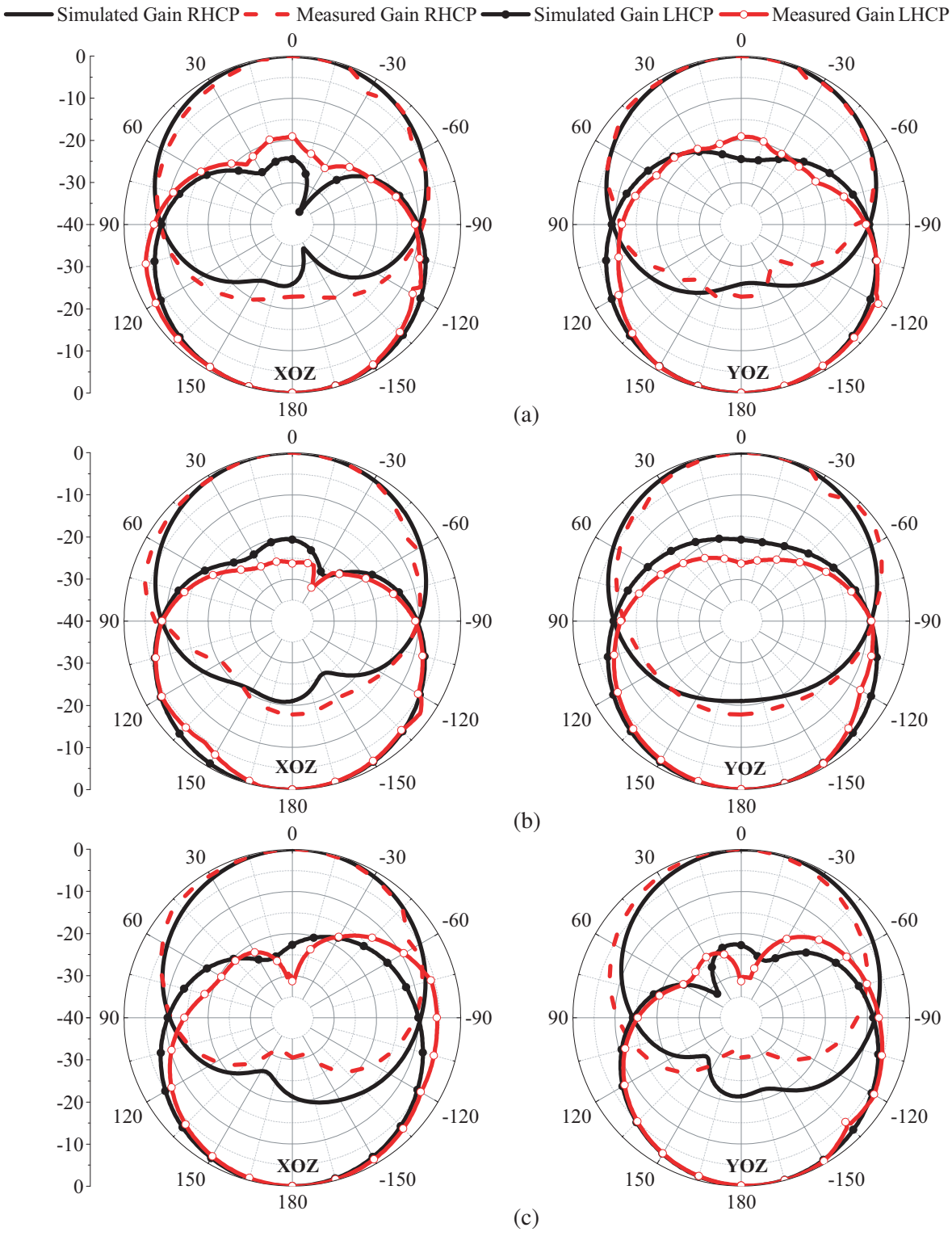


**Figure 5.** Simulated and measured radiation patterns in $XOZ$ and $YOZ$ plane at three typical GNSS bands. (a) GPS L5, (b) BDS B3, and (c) BDS B1.

The antenna has a measured gain at boresight between 2.8 dBic and 4.2 dBic over the 3-dB ARBW. For multi-mode GNSS applications, we read from the measurement that gains at GPS L5, BDS B3, and BDS B1 are 3.1 dBic, 3.0 dBic, and 3.8 dBic, respectively.

Figure 5 depicts the normalized radiation patterns at GPS L5, BDS B3, and BDS B1, which represent the low, middle, and high frequencies of GNSS bands, respectively. Both the simulation and measurement results indicate that the antenna essentially holds constant and symmetric patterns across the GNSS bands. For the prototype antenna, the gain of right-hand circular polarization (RHCP) is larger than the left-hand in $+Z$ direction, demonstrating again that a right-hand circular polarization is realized.

### 3.2. Antenna Phase Response

For each GNSS band, the MPC can be found in the simulation software, by evaluating the phase pattern over the near-hemisphere region of $\theta$ from $-80°$ to $80°$ and $\varphi$ from $0°$ to $360°$. The MPCs for all the 11 GNSS bands are listed in Table 2. The common MPC for the whole GNSS bands can be acquired by averaging the MPCs of the 11 GNSS bands, which is located at (0.7 mm, 2.7 mm, 8.1 mm).

To demonstrate the phase center stability at a single band, we may analyze the PCV of BDS B1 for example. The phase pattern with respect to the MPC at (−0.5 mm, 2.0 mm, 10.3 mm) is presented in Fig. 6. Fig. 6(a) shows the PCV for several specific azimuth angles, and Fig. 6(b) for several specific elevation angles. We find that the PCV keeps within 5°, which indicates a stable phase center over 10° elevation region. Compared to the PCV for GPS bands reported in [11], the proposed antenna has lower phase center variation within a single band, relative to the corresponding MPC.

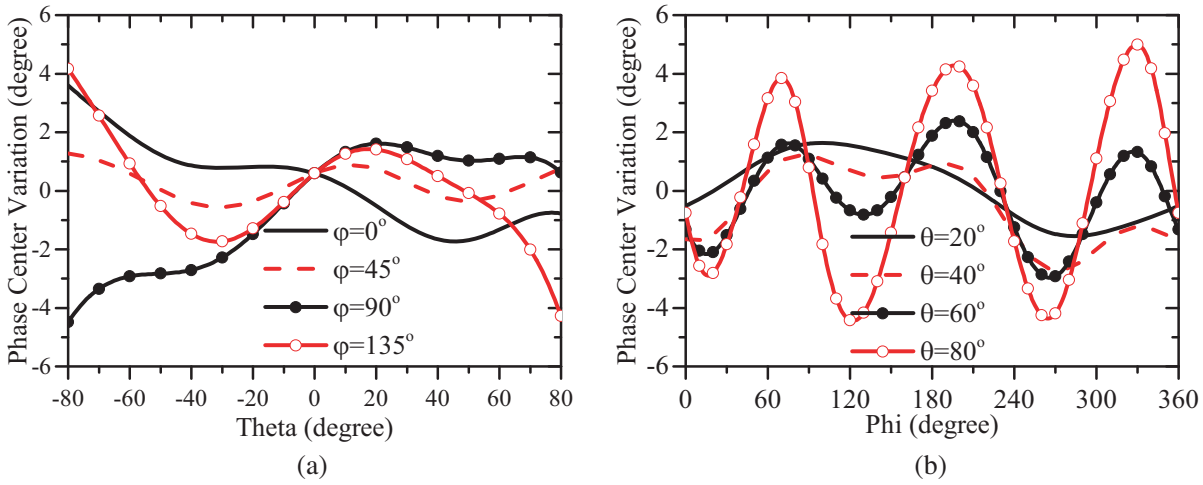


**Figure 6.** Phase center variation with respect to BDS B1 band. (a) Along elevation and (b) along azimuth.

**Table 2.** Mean phase center at GNSS bands (unit: mm).

| GPS L1 | GPS L2 | GPS L5 | BDS B1 |
|---|---|---|---|
| $(-1.0, 2.8, 9.9)$ | $(1.1, 2.5, 7.0)$ | $(0.9, 2.8, 7.2)$ | $(-0.5, 2.0, 10.3)$ |
| BDS B2 | BDS B3 | GLONASS L1 | GLONASS L2 |
| $(1.1, 2.9, 6.8)$ | $(1.2, 2.5, 7.5)$ | $(0, 3.0, 11.1)$ | $(1.5, 2.5, 8.1)$ |
| GLONASS L3 | Galileo E4a/E5b | Galileo E6 | |
| $(1.3, 3.1, 7.1)$ | $(0.9, 2.9, 6.4)$ | $(1.1, 2.8, 7.7)$ | |

To demonstrate the phase center stability with respect to the common MPC, phase patterns of GPS L5, BDS B3 and BDS B1 are shown in Fig. 7. We find that the PCV for these bands retains within 6°. Compared to the PCV for GPS bands reported in [11], the proposed antenna has lower PCV within a broadband, relative to the common MPC. Therefore, the common MPC can be used as the phase center for the whole GNSS bands, benefiting antenna calibration in practice.

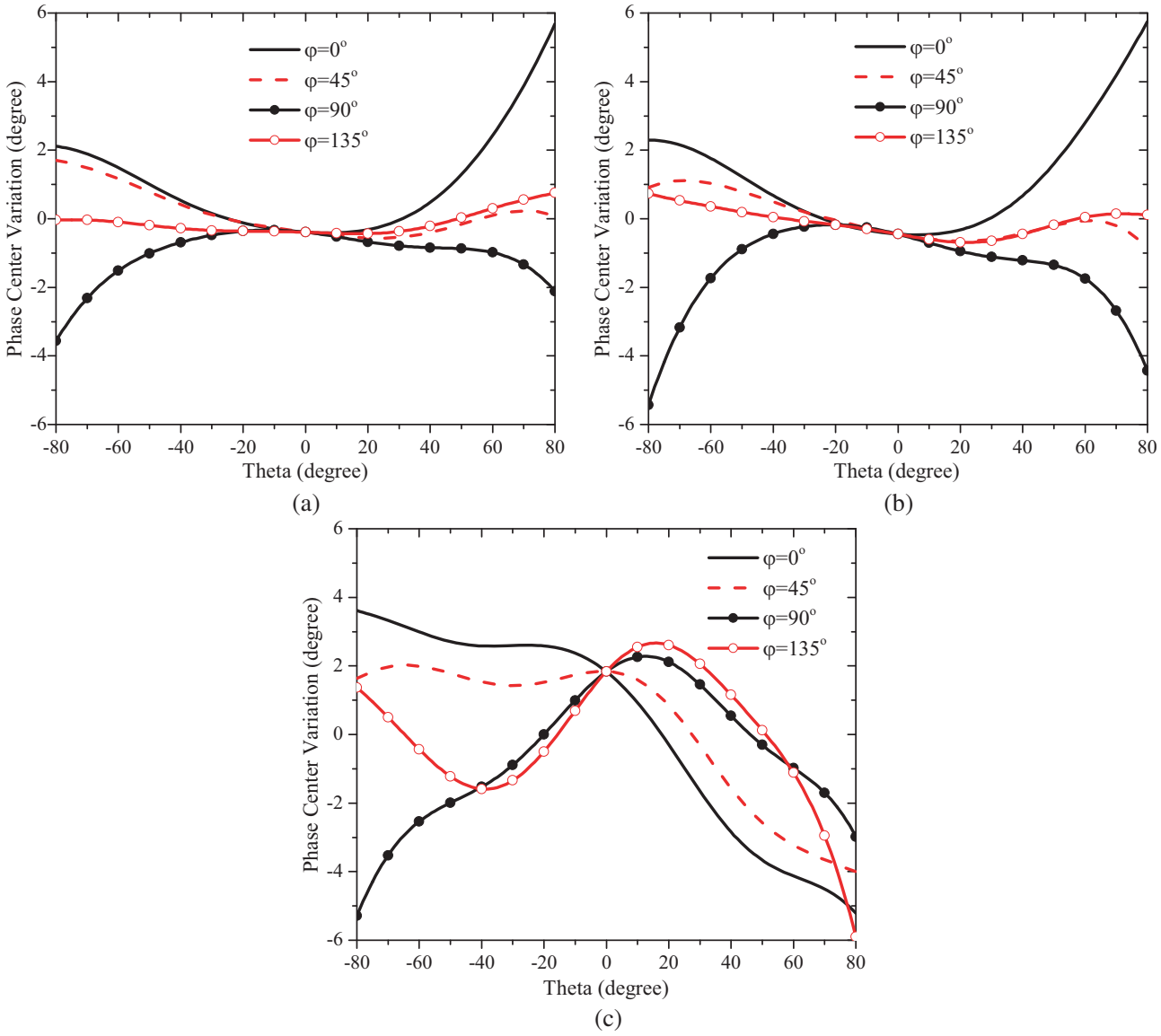


**Figure 7.** Phase center variation with respect to the common MPC at three typical GNSS bands. (a) GPS L5, (b) BDS B3, and (c) BDS B1.

To give an illustrative show of the improvement of phase fluctuation with respect to the MPC, Fig. 8(a) depicts the phase patterns evaluated with the geometry center of the antenna as reference point, while Fig. 8(b) depicts the phase patterns evaluated with the corresponding MPC at each GNSS band as reference point. In Figs. 8(a) and (b), three typical GNSS bands, viz., GPS L5, BDS B3, and BDS B1, are chosen for demonstration. It is observed that the phase fluctuation decreases greatly after choosing the MPC as reference point. Therefore, we can conclude that the proposed antenna achieves stable phase center over 10° elevation region, covering the whole GNSS bands, where PCV keeps below 5°.

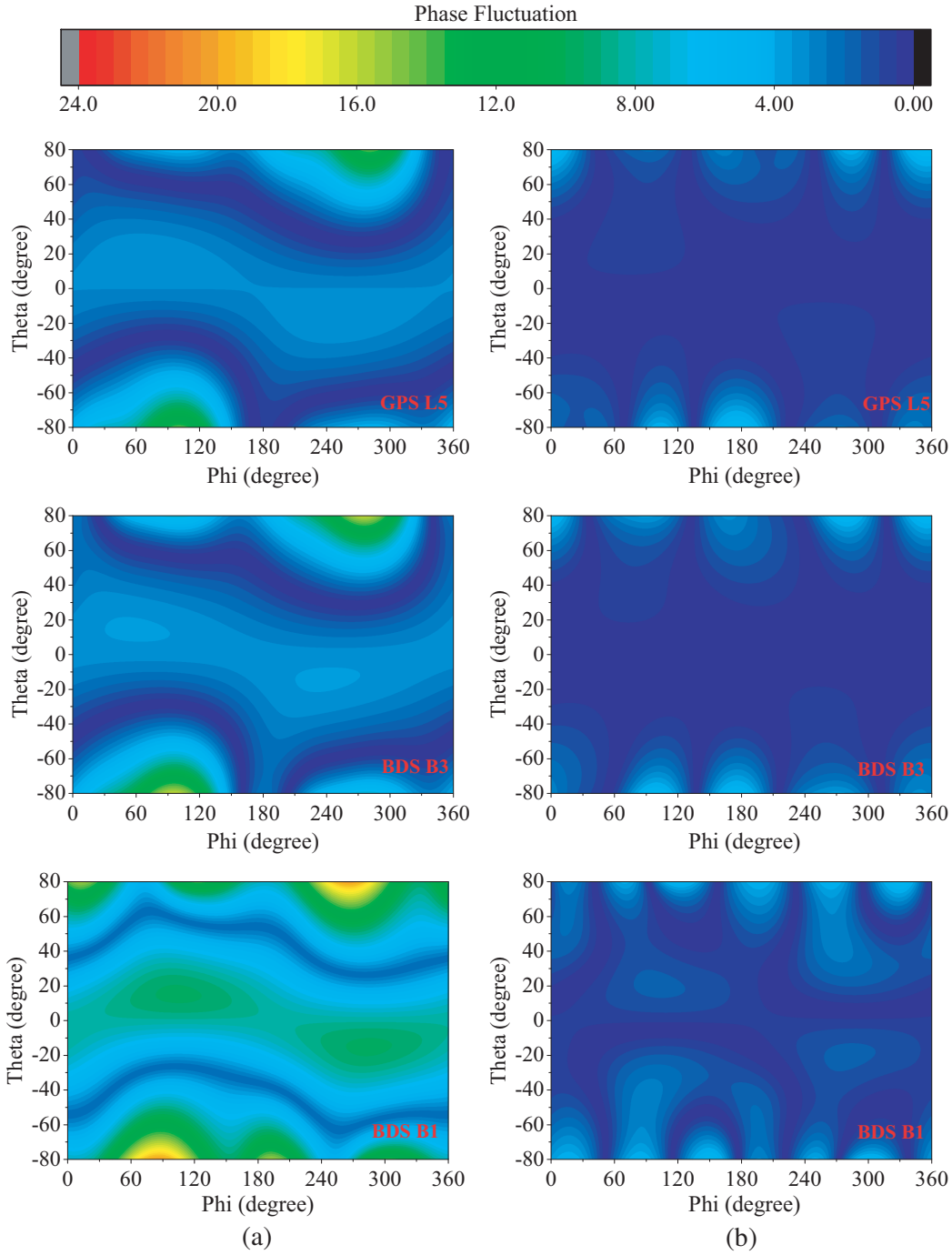


**Figure 8.** Phase fluctuation at three typical GNSS bands with respect to (a) the geometry center of ground and (b) the MPC.

## 4. DISCUSSION

### 4.1. The Mechanism of Circular Polarization Realization

The crossed slots function as a pair of orthogonal dipoles generates the orthogonal electric field modes for circular polarization. For demonstration, we choose parameter L2 to analyze the effects on 3-dB ARBW. Fig. 9(a) depicts the axial ratio of antenna as L2 changes from 70.1 mm to 79.1 mm. Figs. 9(b)

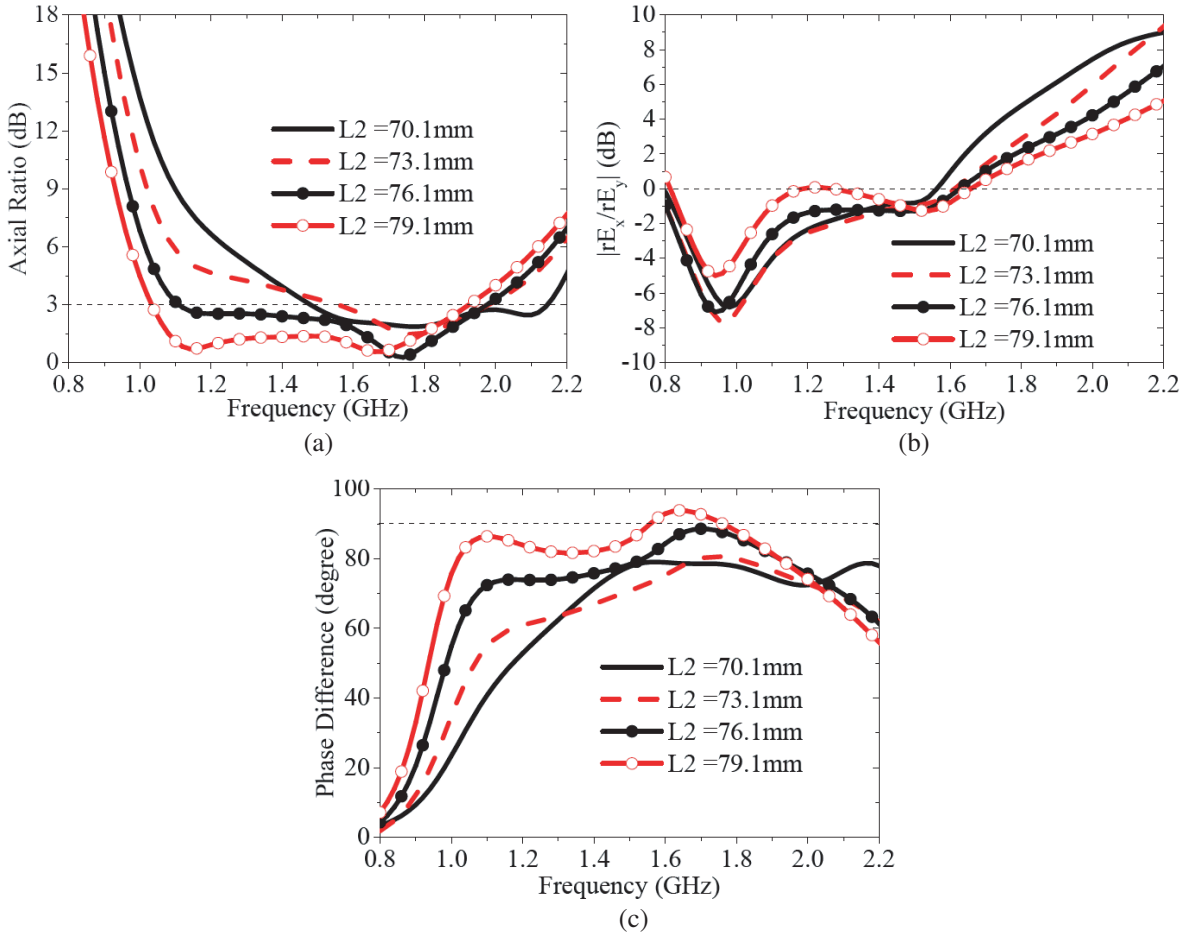


**Figure 9.** Effects of L2 on ARBW-related characteristics. (a) Axial ratio, (b) field strength ratio, and (c) phase difference.

and (c) show the field strength ratio and phase difference of $E_x$ and $E_y$, respectively. We find that L2 may serve as an adjuster for CP realization by tuning the magnitude and phase difference of the orthogonal modes.

### 4.2. Crossed-Slot Antenna with Unidirectional Radiation

We remark that the crossed slots yield a bidirectional radiation. When undirectional radiation is required, a package containing foam of thickness of 30 mm and absorbing material (ECCOSORB MCS) of thickness of 3.5 mm can be added under the antenna to realize undirectional radiation, shown in Fig. 10. Note that undirectional radiation is achieved without modifying the design parameters. Electrical parameters of the absorbing material are plotted in Fig. 11(a). Figs. 11(b) and (c) depict the $S_{11}$ and axial ratio with and without absorbing material. We read from the results that $S_{11}$ and axial ratio are below $-10$ dB and 3 dB, respectively, across the whole GNSS bands, indicating that the absorbing material has limited effects on antenna performance. In Fig. 11(d), we show the antenna gain at $+Z$ and $-Z$ direction with absorbing material, and it is observed that the forward radiation is much larger than the backward radiation, demonstrating that an undirectional radiation is realized.

### 4.3. Comparison

Performance comparisons between the designed antenna and other broadband GNSS antennas are listed in Table 3. We note that the antennas reported in [15–17] cover most part of the GNSS bands. Compared

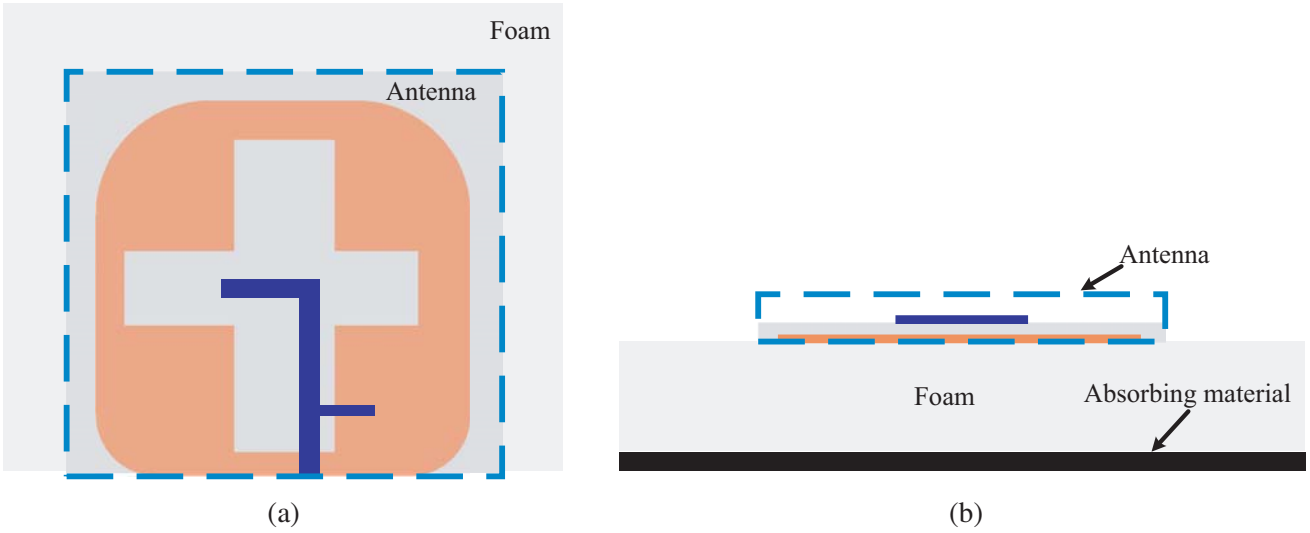


**Figure 10.** Antenna configuration with unidirectional radiation. (a) Top view, (b) side view.

to other broadband CP antennas for GNSS applications, the proposed antenna has a more compact size, where $\lambda_0$ represents the wavelength at the lowest pass band. Since no phase center stability in the whole GNSS bands was stressed in other designs, comparison of phase center stability is not included in Table 3.

**Table 3.** Comparison of broadband GNSS antennas.

| Ref. | −10-dB IBW (%, GHz) | 3-dB ARBW (%, GHz) | Feeding port (single/multiple) | Size ($\lambda_0^2$) |
|---|---|---|---|---|
| [14] | > 42.9 (> 1.1–1.7) | 42.9 (1.1–1.7) | Multiple | 0.45 × 0.45 |
| [15] | 31.3 (1.4–1.92) | 16 (1.51–1.77) | Multiple | 0.51 × 0.51 |
| [16] | 25.5 (1.37–1.77) | 21.8 (1.47–1.83) | Single | 0.34 × 0.34 |
| [17] | 66.2 (1.01–2.01) | 47.8 (1.21–1.97) | Multiple | 0.40 × 0.40 |
| [18] | 35.6 (1.13–1.62) | 35.4 (1.14–1.63) | Single | 0.30 × 0.30 |
| This work | 76.7 (0.9–2.02) | 64.0 (1.03–2.0) | Single | 0.30 × 0.29 |

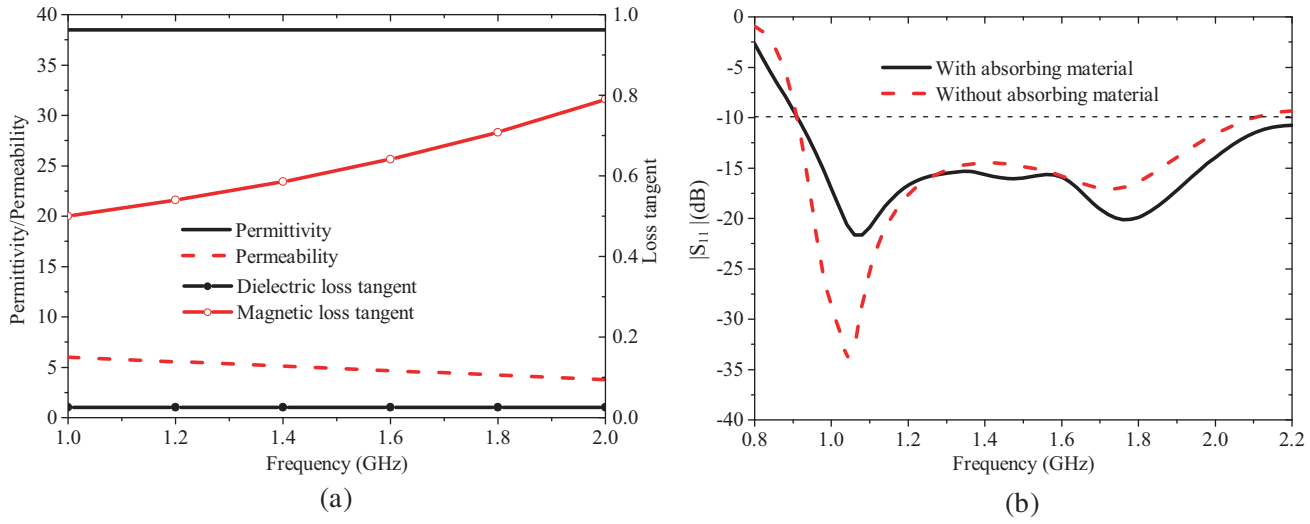

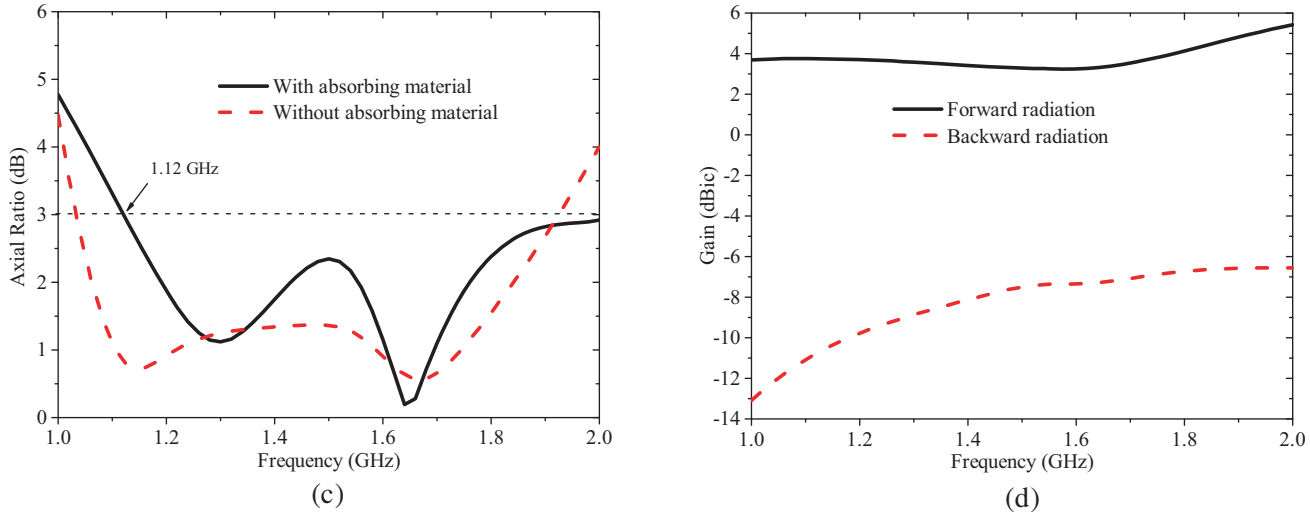


**Figure 11.** Antenna performance with unidirectional radiation. (a) Electrical parameters of the absorbing material, (b) $S_{11}$, (c) axial ratio, and (d) gain at $+Z$ and $-Z$ direction.

## 5. CONCLUSION

This paper proposes a design of broadband CP antenna with stable phase center for the whole GNSS bands. Both simulation and measurement of the designed antenna demonstrate a −10-dB impedance bandwidth of 76.7% and a 3-dB axial ratio bandwidth of 64%, which cover all GPS, BeiDou, Galileo, and GLONASS bands ranging from 1.164 GHz to 1.612 GHz. In addition, stable phase center for orientation in the region above 10° elevation is realized for high-precision positioning. For each GNSS band, phase center variation with respect to its own mean phase center can be retained within 5°. Over the whole GNSS bands, phase center variation with respect to the common mean phase center is retained within 6°.

## ACKNOWLEDGMENT

This work was supported in part by the National Natural Science Foundation of China under Grant 61671421. The authors would like to thank the Information Science Laboratory Center of USTC for the antenna measurement.

## REFERENCES

1. Hegarty, C. J. and E. Chatre, "Evolution of the global navigation satellite systems (GNSS)," *Proc. IEEE*, Vol. 96, No. 22, 1902–1917, 2008.
2. Kumar, A., A. Sarma, E. Ansari, and K. Yedukondalu, "Improved phase center estimation for GNSS patch antenna," *IEEE Trans. Antennas Propag.*, Vol. 61, No. 4, 1909–1915, 2013.
3. Jan, J.-Y. and J.-W. Su, "Bandwidth enhancement of a printed wide-slot antenna with a rotated slot," *IEEE Trans. Antennas Propag.*, Vol. 53, No. 6, 2111–2114, 2005.
4. Sze, J.-Y. and S.-P. Pan, "Design of broadband circularly polarized square slot antenna with a compact size," *Progress In Electromagnetics Research*, Vol. 120, 513–533, 2011.
5. Mousavi, P., B. Miners, and O. Basir, "Wideband L-shaped circular polarized monopole slot antenna," *IEEE Antennas Wireless Propag. Lett.*, Vol. 9, 822–825, 2010.
6. Jan, J.-Y., C.-Y. Pan, K.-Y. Chiu, and H.-M. Chen, "Broadband CPW-fed circularly polarized slot antenna with an open slot," *IEEE Trans. Antennas Propag.*, Vol. 61, No. 3, 1418–1422, 2013.

7. Ellis, M. S., Z. Zhao, J. Wu, X. Ding, Z. Nie, and Q.-H. Liu, "A novel simple and compact microstrip-fed circularly polarized wide slot antenna with wide axial ratio bandwidth for C-band applications," *IEEE Trans. Antennas Propag.*, Vol. 64, No. 4, 1552–1555, 2016.
8. Best, S. R., "Distance-measurement error associated with antenna phase-center displacement in time-reference radio positioning systems," *IEEE Antennas Propag. Mag.*, Vol. 46, No. 2, 13–22, 2004.
9. Mania, L., "The antenna phase center in satellite radio Doppler geodetic systems," *IEEE Trans. Geosci. Remote Sens.*, Vol. GE-20, No. 4, 536–543, 1982.
10. Tranquilla, J. M. and B. G. Colpitts, "GPS antenna design characteristics for high-precision applications," *Journal of Surveying Engineering*, Vol. 115, No. 1, 1989.
11. Wang, J. H., "Antennas for Global Navigation Satellite Systems (GNSS)," *Proc. IEEE*, Vol. 100, No. 7, 2349–2355, 2012.
12. Zheng, K.-K. and Q.-X. Chu, "A small symmetric-slit shaped and annular slotted BeiDou antenna with stable phase center," *IEEE Antennas Wireless Propag. Lett.*, Vol. 17, 146–149, 2018.
13. Zheng, K.-K. and Q.-X. Chu, "A novel annular slotted center-fed BeiDou antenna with stable phase center," *IEEE Antennas Wireless Propag. Lett.*, Vol. 17, 364–367, 2018.
14. Li, D., P. F. Guo, Q. Dai, and Y. Q. Fu, "Broadband capacitively coupled stacked patch antenna for GNSS applications," *IEEE Antennas Wireless Propag. Lett.*, Vol. 11, 701–704, 2012.
15. Fu, S., Q. Kong, S. Fang, and Z. Wang, "Broadband circularly polarized microstrip antenna with coplanar parasitic ring slot patch for L-band satellite system application," *IEEE Antennas Wireless Propag. Lett.*, Vol. 13, 943–946, 2014.
16. Pakkathillam, J. K. and M. Kanagasabai, "Circularly polarized broadband antenna deploying fractal slot geometry," *IEEE Antennas Wireless Propag. Lett.*, Vol. 14, 1286–1289, 2015.
17. Xu, R., J.-Y. Li, and W. Kun, "A broadband circularly polarized crossed-dipole antenna," *IEEE Trans. Antennas Propag.*, Vol. 64, No. 10, 4509–4513, 2016.
18. Wang, K., H.-Y. Tang, R. Wu, and C. Yu, "Compact broadband circularly polarized monopole antenna for Global Navigation Satellite System (GNSS) applications," *Progress In Electromagnetics Research C*, Vol. 69, 27–36, 2016.